RESEARCH ARTICLE

Quantification of Tumor Hypoxic Fractions Using Positron Emission Tomography with [^{18}F]Fluoromisonidazole ([^{18}F]FMISO) Kinetic Analysis and Invasive Oxygen Measurements

Olivia J. Kelada,[1,2] Sara Rockwell,[1,3] Ming-Qiang Zheng,[4] Yiyun Huang,[4] Yanfeng Liu,[1] Carmen J. Booth,[5] Roy H. Decker,[1] Uwe Oelfke,[2] Richard E. Carson,[4] David J. Carlson[1]

[1]Department of Therapeutic Radiology, Yale University School of Medicine, P.O. Box 208040, New Haven, CT, 06520-8040, USA
[2]Department of Medical Physics in Radiation Oncology, German Cancer Research Center, Heidelberg, Germany
[3]Department of Pharmacology, Yale University School of Medicine, New Haven, CT, USA
[4]Department of Diagnostic Radiology, Yale University School of Medicine, New Haven, CT, USA
[5]Section of Comparative Medicine, Yale University School of Medicine, New Haven, CT, USA

Abstract

Purpose: The purpose of this study is to use dynamic [^{18}F]fluoromisonidazole ([^{18}F]FMISO) positron emission tomography (PET) to compare estimates of tumor hypoxic fractions (HFs) derived by tracer kinetic modeling, tissue-to-blood ratios (TBR), and independent oxygen (pO$_2$) measurements.

Procedures: BALB/c mice with EMT6 subcutaneous tumors were selected for PET imaging and invasive pO$_2$ measurements. Data from 120-min dynamic [^{18}F]FMISO scans were fit to two-compartment irreversible three rate constant (K_1, k_2, k_3) and Patlak models (K_i). Tumor HFs were calculated and compared using K_i, k_3, TBR, and pO$_2$ values. The clinical impact of each method was evaluated on [^{18}F]FMISO scans for three non-small cell lung cancer (NSCLC) radiotherapy patients.

Results: HFs defined by TBR ($\geq$1.2, $\geq$1.3, and $\geq$1.4) ranged from 2 to 85 % of absolute tumor volume. HFs defined by K_i (>0.004 ml min cm^{-3}) and k_3 (>0.008 min^{-1}) varied from 9 to 85 %. HF quantification was highly dependent on metric (TBR, k_3, or K_i) and threshold. HFs quantified on human [^{18}F]FMISO scans varied from 38 to 67, 0 to 14, and 0.1 to 27 %, for each patient, respectively, using TBR, k_3, and K_i metrics.

Conclusions: [^{18}F]FMISO PET imaging metric choice and threshold impacts hypoxia quantification reliability. Our results suggest that tracer kinetic modeling has the potential to improve hypoxia quantification clinically as it may provide a stronger correlation with direct pO$_2$ measurements.

Key words: [^{18}F]FMISO, Pet, Tumor, Hypoxia, pO$_2$ electrode, Quantification

Correspondence to: David Carlson; *e-mail:* david.j.carlson@yale.edu

Introduction

Tumor hypoxia correlates with increased metastatic risk and resistance to radiation and chemotherapy [1]. Invasive and non-invasive techniques have been developed to measure tumor hypoxia. Invasive methods, e.g., the Eppendorf pO_2 electrode, provide real-time pO_2 measurements and have shown a correlation between tumor hypoxia and negative patient survival [2, 3]. However, such techniques are user dependent, subject to sampling error, and limited to easily accessible tumors [4].

Non-invasive molecular imaging techniques are increasingly used in the clinic to address limitations of invasive methods [5]. Positron emission tomography (PET) can be used to assess the magnitude and variability of tumor hypoxia and guide treatment decisions [6, 7]. [18F]Fluoromisonidazole ([18F]FMISO) PET [8] is considered one of the more promising hypoxia quantification methods because the tracer selectively binds in hypoxic cells [9–12]. [18F]FMISO is reduced by nitroreductase enzymes and covalently bound to intracellular macromolecules in the absence of oxygen, causing accumulation of F-18 radioactivity in hypoxic cells [13]. Others [9, 10] first demonstrated [18F]FMISO could detect hypoxia in human tumors [11] and showed the biomarker was representative of intracellular pO_2 [14].

Current methods used to quantify the hypoxic fraction (HF), i.e., percentage of the tumor volume defined as hypoxic, do not provide absolute pO_2 values and can lead to highly variable results [5]. Tissue-to-blood ratio (TBR), the most common metric to quantify tumor hypoxia with PET (~1 in normal tissues), is dependent on threshold values (first defined as ≥1.4 [9], ranging from 1.1 to 1.5 in the literature). Others [15, 16] have attempted to identify an [18F]FMISO parameter that correlates with a pO_2 value for the same tumor volume [17].

PET tracer kinetic modeling derives tracer binding parameters from the tissue activity curves of dynamic PET datasets [18]. Thorwarth et al. [19] and others [20, 21] suggested kinetic modeling could provide more accurate tumor hypoxia quantification accounting for both delivery of tracer to tumor (K_1) and binding to hypoxic cells (k_3) [19]. Bartlett et al. [22] compared these parameters with TBR and determined that k_3 was the most accurate hypoxic quantifier. However, it remains unclear which metric or threshold is the most clinically relevant, and the method of image analysis could impact biological treatment planning and treatment outcomes analysis.

We assess the impact of different PET imaging metrics (TBR and kinetic parameters) and thresholds on the accuracy of tumor HF quantification and correlate these parameters with independent pO_2 measurements.

Methods and Materials

Animal and Tumor Models

EMT6 mouse mammary carcinoma cells were grown *in vitro* and 2×10^5 cells were injected subcutaneously into the right-upper limb of all six male BALB/c mice (average weight ~30 g) aged ≥2 months. Imaging was performed ~2 weeks post-inoculation when tumors were ~0.6 cm^3. Murine experimental protocols were approved by the Yale University Institutional Animal Care and Use Committee and conducted in full compliance with the Association for the Assessment and Accreditation of Laboratory Animal Care, governmental and institutional regulations, and principles outlined in the United States Public Health Service Guide. After completion of all experiments, mice were euthanized under anesthesia by cervical dislocation.

Cell line information, including origin, characteristics, growth methods, and presence of tumor hypoxia, is described elsewhere [23–27]. Others ([4, 28]) have characterized the use of this subcutaneous model for tumor hypoxia measurement with pO_2 probes and PET imaging.

PET Imaging

Preclinical Imaging Mice were anesthetized with isoflurane and air and injected i.v. with [18F]FMISO (maximum 0.5 mCi). [18F]FMISO was prepared according to previously published methods [29]. Animals underwent a whole-body 120-min dynamic PET scan using a microPET scanner (Focus 220, Siemens, U.S.A.). A transmission scan was acquired for attenuation correction and computed tomography (CT) for registration purposes. Rodents were transferred from the microPET (in the same immobilized position) on a removable tray to the microSPECT-CT scanner (X-SPECT, GammaMedica-Ideas, Northridge, CA) for CT imaging.

List mode data were binned as follows: 6 × 30 s and 3 × 1, 2 × 2, and 22 × 5 min. Dynamic PET images were reconstructed into a 256 × 256 × 95 matrix (voxel dimensions, 0.949 × 0.949 × 0.796 mm) using Fourier rebinning followed by filtered back projection algorithm with a ramp filter. Corrections for attenuation, scatter, randoms, and dead time were applied to each frame.

Clinical Imaging Human [18F]FMISO PET/CT scans were acquired on a Siemens Biograph mCT scanner (Siemens Medical Solutions, Hoffman Estates, Knoxville, TN, USA) in patients with early stage non-small cell lung cancer (NSCLC) tumors. Each [18F]FMISO PET scan consisted of three parts, acquired dynamically from 0 to 120, 150–180, and 210–240 min post-injection. A CT was performed before each part for attenuation correction. List mode data were divided into frames of 6 × 30 s and 3 × 1, 2 × 2, and 33 × 5 min. Dynamic PET images were reconstructed into a 400 × 400 × 111 matrix (voxel dimensions, 2.036 × 2.036 × 2 mm) using a OP-OSEM, PSF, and TOF with a 3.0-mm FWHM Gaussian isotropic filter, 2-mm isotropic voxels, and no zoom. Global dead time and model-based scatter correction was also carried out for each frame.

Preclinical and Clinical [^{18}F]FMISO PET Analysis

Input Function and ROI Definition MEDx 7.1 (Medical Numerics, Sterling, VA) and MATLAB (Mathworks Inc, Natick, MA) were used for image visualization and processing. Image-derived input functions were identified by drawing a region of interest (ROI) on the PET transaxial slices containing the heart in frames acquired <2–5 min post-injection. The heart ROI was then applied to the whole dynamic PET dataset to generate an input function using the average activity in the heart ROI. The heart time-activity curve (TAC), after its peak, was fitted using a sum of exponential functions (1 to 3 exponentials, automatically determined by minimizing the chi-square criterion) to reduce noise for more accurate kinetic analysis.

For preclinical imaging, tumor and muscle ROIs were drawn on CT and co-registered to PET images using FLIRT (Oxford UK) [30, 31] to perform a linear six-parameter rigid registration based on mutual information. Absolute tumor volume was verified using caliper measurement after tumor excision. For clinical imaging, the absolute tumor volume was created by the radiation oncologist contouring the tumor ROI on CT. The tumor diameter was measured on the treatment planning CT.

Calculation of Tissue-to-Blood Ratio and Hypoxic Fraction Uptake values in each tumor ROI voxel were divided by the average value in the heart ROI from 90 to 120 min post-injection (preclinical) and 210–240 min post-injection (clinical) to create a TBR value for each voxel. Values were averaged to give a mean TBR for the tumor ROI, and a threshold was applied to calculate the percentage of tumor voxels that were hypoxic, i.e., above the defined threshold.

Voxel-by-Voxel Tumor Kinetic Analysis A two-tissue compartment (2TC) model was used to generate tracer kinetic parameters [22]. Kinetic parameters K_1 (ml min cm^{-3}), k_2 (min^{-1}), and k_3 (min^{-1}) were averaged over the whole tumor and estimated for each voxel. Relevant parameters were k_3 and K_i ($K_1k_3/(k_2 + k_3)$), the net rate of tracer binding and influx, respectively. Levenberg–Marquardt least-squares optimization algorithm was used to estimate model parameters in each voxel. In addition, Patlak analysis was performed to provide K_i only [32].

HFs were quantified using different individual imaging metrics (TBR, k_3, or K_i) and thresholds (1.2, 1.3, 1.4 for TBR, 0.008 min^{-1} for k_3, and 0.004 ml min cm^{-3} for K_i). Variation in HF across these metrics and thresholds for TBR was assessed by comparing the median HF across all mice. Parametric maps were visualized in MATLAB. For clinical imaging, HF was defined as the percentage of the absolute tumor volume exhibiting a TBR >1.2 and >1.4, k3 >0.008 min^{-1}, and Ki >0.004 ml min cm^{-3}.

Preclinical pO$_2$ Measurements

Partial oxygen pressure (pO$_2$) was measured with an Eppendorf pO$_2$ histograph. (Eppendorf KIMOC 6650, Hamburg, Germany) [33]. Needle trajectories were guided using plastic grids [three per row and 1 mm apart]. A 0.5-mm step length of needle was set (~half the size of a PET voxel) by advancing 0.8 mm and retracting 0.3 mm to avoid inaccuracy due to needle tip pressure. Forty pO$_2$ tumor measurements (four tracks of ten measurements each) and 30 pO$_2$ anterior right leg muscle measurements (three tracks of ten measurements each) were acquired. Distributions of measured values were plotted as histograms to compare tumor and muscle readings (as reference normoxic tissue with a pO$_2$ range of 20–40 mmHg). Mean pO$_2$ values were calculated.

Preclinical pO$_2$ Measurement Analysis and Parametric Image Comparison

Parametric maps (TBR, k_3 and K_i) were created using in-house software and ROI values were imported into GraphPad (La Jolla California USA). Four tumor ROI regions were selected (to reduce sampling error) to spatially correspond to pO$_2$ readings based on external grid placement. Two track readings corresponded to PET voxel width. To reduce the impact of spatial registration error between PET voxel location and electrode placement, measured pO$_2$ values were averaged to calculate mean pO$_2$ across all tumor and muscle voxels and correlated with mean TBR, k_3, or K_i voxel values for the same approximate spatial tumor or muscle area. Kinetic parameter thresholds k_3 = 0.008 min^{-1} and K_i = 0.004 ml min cm^{-3} were selected to yield comparable HF values as TBR >1.2.

Statistical Methods

The median imaging metric value was calculated for tumor and muscle ROIs for all mice. An assessment of the difference of the medians was done using a Wilcoxon ranksum test ($p < 0.05$) [34]. R^2 values were calculated and used to analyze how differences in [^{18}F]FMISO PET metrics can be explained by a difference in a pO$_2$ using the correlation plots. Standard deviation (SD) was calculated for each metric to provide the uncertainty in HF estimation.

Results

Figure 1 shows histograms of mouse tumor and muscle pO$_2$ values. Mean tumor pO$_2$ values ranged between 1 and 9 mmHg and mean muscle values between 21 and 35 mmHg. Mean tumor and mean muscle pO$_2$ values were within expected ranges, 0–10 mmHg for tumor and 20–60 mmHg for muscle. Muscle values <20 mmHg are attributed to
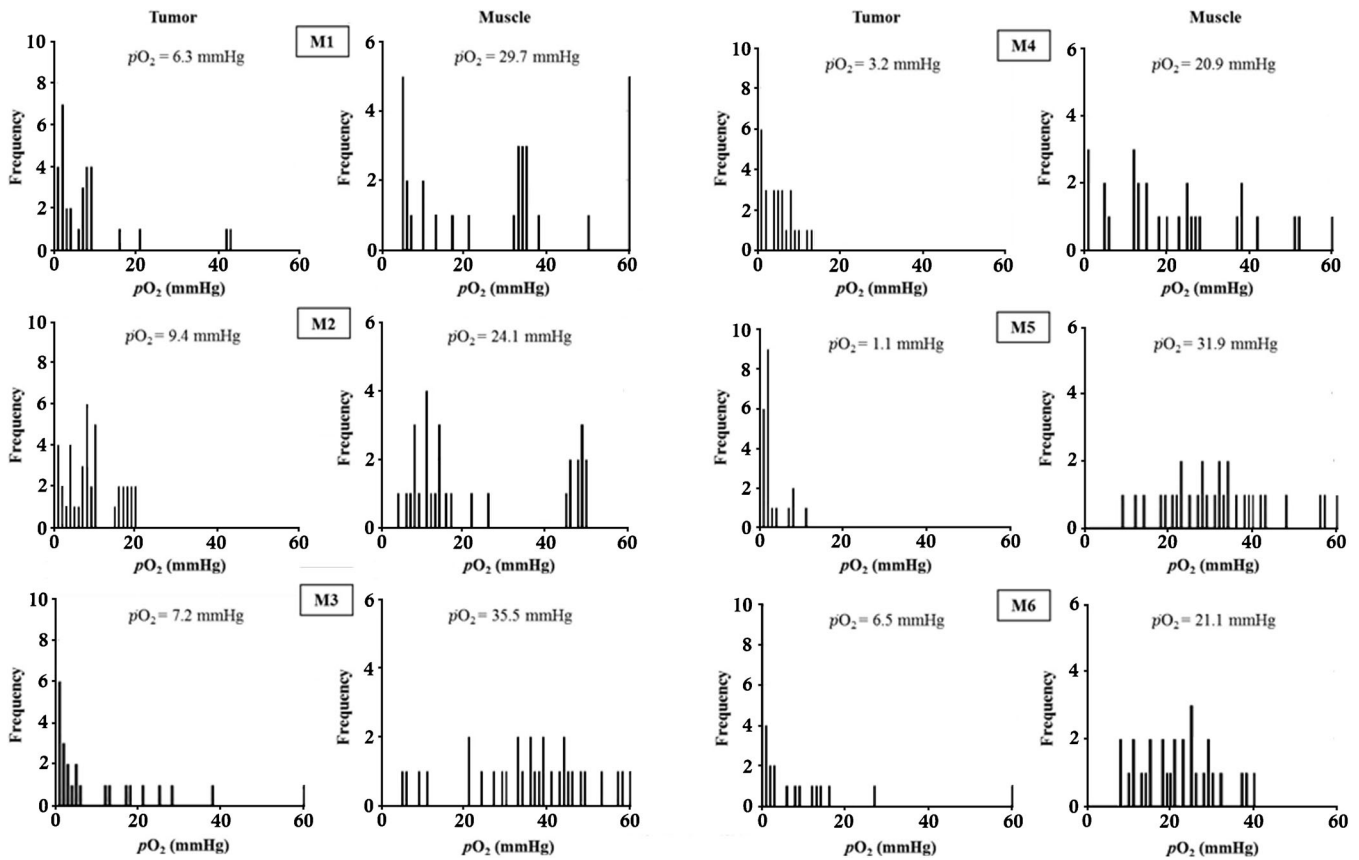
Fig. 1. Histograms showing measured pO_2 values for mouse tumors and muscles (*M1–M6*). Mean tumor pO_2 values range between 1.1 and 9.4 mmHg and mean muscle values between 20.9 and 35 mmHg.

prolonged time under anesthesia and possible probe mis-placement into nearby fascia or fatty tissue.

Table 1 shows tumor HFs as defined by TBR thresholds >1.2, >1.3, and >1.4 and Patlak and 2TC rate constants. The median HFs for mouse 1–6 (M1–M6) using TBR >1.2, 1.3, and 1.4 were 43, 29, and 19 %, respectively, a variation of up to a factor of 1.5. Compared to median HFs defined by 2TC k_3, K_i, and Patlak K_i, these were 39, 57, and 54 %, respectively, varying by up to a factor of 1.5. Variation of up to a factor of 3 was observed between median HFs

calculated by TBR versus kinetic modeling parameters. Median HF using pO_2 <5 mmHg (a commonly accepted threshold for radiobiological hypoxia [35, 36]) was 71 %, a value up to 3.5 times larger when compared to median HF calculated by TBR and kinetic parameter thresholds.

Figure 2 shows transaxial images ($n = 6$) highlighting the visual differences in HFs by comparing TBR values estimated from static late PET images with kinetic parameters derived from the entire dynamic scan (display range shows hypoxia as white, tumor location indicated with

Table 1. Comparison of hypoxic fractions for each tumor using TBRs and rates of tracer influx (K_i in ml/min/g) and binding (k_3 in min^{-1}) for 2TC and Patlak models. Error is shown as ± standard deviation for each metric

| Mouse	Hypoxic fraction (%)						
	pO_2 <5 mmHg	TBR >1.2	TBR >1.3	TBR >1.4	$k_3 > 0.008$ (2TC)	$K_i > 0.004$ (2TC)	$K_i > 0.004$ (Patlak)
M1	60 ± 3.9	1.97 ± 3.1	0 ± 3.1	0 ± 3.1	11.0 ± 7.5	13.8 ± 3.6	13 ± 2.7
M2	30 ± 2.4	27.6 ± 0.4	11.1 ± 0.4	2.93 ± 0.4	52.5 ± 4.7	60.4 ± 1.4	53.4 ± 1.1
M3	70 ± 3.8	58.3 ± 0.7	47.8 ± 0.7	34.6 ± 0.7	35.2 ± 2.7	54 ± 0.9	54.9 ± 0.7
M4	67.5 ± 1.6	84.8 ± 1.7	77.8 ± 1.7	67.1 ± 1.7	42.4 ± 3.4	63.3 ± 1.0	71.5 ± 0.7
M5	90 ± 1.2	10.6 ± 0.4	5.3 ± 0.4	0 ± 0.4	12.9 ± 0.6	22 ± 0.6	9.09 ± 0.4
M6	77.5 ± 2.6	84.1 ± 1.8	73.1 ± 1.8	61.9 ± 1.8	72.9 ± 2.4	85.3 ± 2.4	80.4 ± 1.8
Mouse		Absolute vol. (cm3)	Mean pO2 (mmHg)	Mean TBR	Mean k_3 (2TC)	Mean K_i (2TC)	Mean K_i (Patlak)
M1		1.14	6.26	0.82	0.0036	0.0019	0.0016
M2		0.44	9.37	1.12	0.0129	0.0047	0.0041
M3		0.29	2.30	1.24	0.0071	0.0047	0.0049
M4		0.29	3.19	1.55	0.0082	0.0057	0.0071
M5		0.17	1.10	1.00	0.0040	0.0025	0.0017
M6		0.65	4.03	1.45	0.0121	0.0068	0.0064
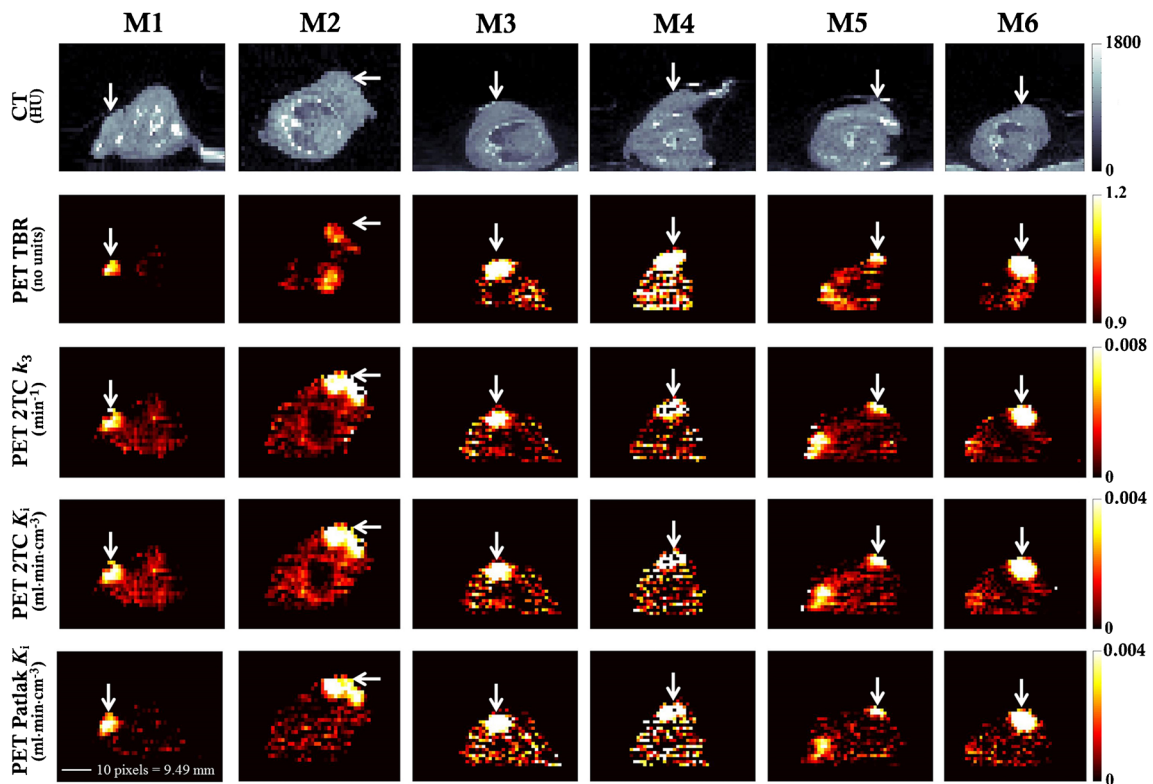
Fig. 2. Axial images (*M1–M6*) showing HF variations: *Row (1)* CT. (*2*) 90–120 summed PET, TBR >1.2 shows hypoxia. (*3*), (*4*), and (*5*) Parametric map of k_3 min^{-1} (2TC), threshold = 0.008 min^{-1}; parametric map of K_i (ml min cm^{-3}), threshold = 0.004 ml min cm^{-3}, 2TC; and Patlak, respectively. *Arrows* indicate tumor hypoxia, and *scale bar* on the *right* shows hypoxia as *white*.

arrows). Each column corresponds to one mouse (M1–M6). Row (1) shows the CT images of a representative mouse tumor slice. Subsequent rows show PET images created using different [^{18}F]FMISO imaging metrics. Row (2) shows TBR (>1.2) images calculated using 90–120 summed image. Rows (3), (4), and (5) show parametric images for k_3 (>0.008), K_i 2TC (>0.004), and Patlak K_i (>0.004) respectively.

Figure 3 shows the correlation between mean tumor and muscle pO_2 and mean imaging metrics for tumor hypoxia (TBR, k_3, and K_i). An inverse relationship was observed between mean pO_2 and mean [^{18}F]FMISO values. Data were fit using an exponential function ($Y = Y0*\exp(K*X)$, $X = pO_2$), which provided a reasonable empirical description of the data (Y0 = 1.464, 0.013, 0.007 and 0.008 and K = −0.018, −0.044, −0.046, and −0.046 for TBR, k_3, 2TC K_i, and Patlak K_i, respectively). R^2 values from this function fit were 0.25, 0.25, 0.30, and 0.32 for TBR, k_3, 2TC K_i, and Patlak K_i, respectively. For low pO_2 values, a high k_3, high K_i, and high TBR were observed. The fit for the K_i Patlak metric yielded the highest R^2 value of 0.32.

An assessment of the difference of the medians was done using a Wilcoxon rank-sum test ($p < 0.05$, corrected for multiple comparisons). The median values for all [^{18}F]FMISO imaging metrics (TBR, k_3, and K_i) for the tumor, and muscle pO_2 groups for all mice were compared. For k_3, K_i (2TC), and K_i (Patlak),

the p values were 0.0043, 0.0043, and 0.0043, respectively, and all statistically significant ($p \leq 0.05$). No statistically significant difference was observed between the tumor and muscle TBR values, suggesting that model-based methods are more sensitive. Figure 4 (a–d) shows a voxel-by-voxel correlation of imaging metrics (TBR, k_3 and K_i) and pO_2 values for one mouse tumor, as described by $Y = Y0*\exp(K*X)$ where Y0 = 1.00, 0.004, 0.01, and 0.005 and K = -0.003, -0.04, -0.13, and -0.13 and R2 values were 0.02, 0.24, 0.42 and 0.39 or a, b, c, and d, respectively. Again, an inverse relationship was observed between pO_2 and mean [^{18}F]FMISO values. Figure 4 e-h shows the correlation between mean tumor pO_2 and mean imaging metrics for tumor hypoxia (TBR, k_3 and K_i) for all mice (M1–M6). A solid line indicates the fit of a nonlinear inverse-exponential described by $Y = Y0*\exp(K*X)$. R^2 values were 0.04, 0.25, 0.15, and 0.08. Error bars are standard deviations of the mean for each [^{18}F]FMISO metric. Due to the small sample size of the tumor data, the under-sampling of the pO2 probe, and additional factors outlined in the discussion, the correlation without the muscle data is not consistent with physiological expectations.

Figure 5 shows the clinical impact of imaging metric and threshold on HF quantification in human tumors with [^{18}F]FMISO PET imaging. In patient A, HFs were estimated as 67, 52, 41, and 38 % of total tumor volume using TBR >1.2, TBR >1.4, k_3 > 0.008, and K_i > 0.004, respectively. In
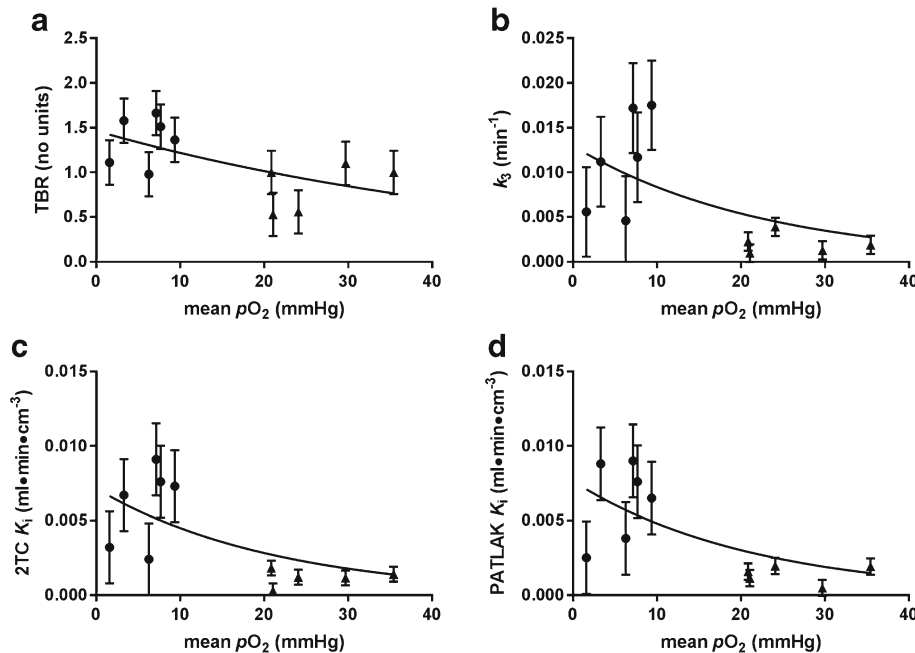
Fig. 3. *Symbols* show mean tumor (*circle*) or muscle (*triangle*) PET imaging metric and mean tumor or muscle pO_2 for each mouse (M1–M6). *Solid lines* indicate inverse-exponential relationship between mean pO_2 (by Eppendorf electrode) and [^{18}F]FMISO parameter described by $Y = Y0*exp(K*X)$ where Y0 = 1.464, 0.013, 0.007, and 0.008 and K = −0.018, −0.044, −0.046, and −0.046 and for **a**, **b**, **c** and **d**, respectively. **a** TBR, **b** k_3, **c** 2TC K_i, and **d** Patlak K_i. R^2 values were 0.25, 0.25, 0.30, and 0.32, respectively. *Error bars* are standard deviations of the mean for each [^{18}F]FMISO metric.

patients B and C, HFs were estimated to as 14, 1.6, 0, and 0 % and 27, 7.4, 1.2, and 0.1 %, respectively, using the same metrics. The variation in HF in all three patients highlights the importance of metric and threshold choice in the use of [^{18}F]FMISO PET imaging for radiation therapy applications. For example, the yellow contours in each panel could be used as a biological target volume that would receive a higher radiation prescription dose than the surrounding tumor volume.

Discussion

In this work, several PET imaging metrics (including kinetic model-derived metrics) used to quantify tumor hypoxia were directly compared and correlated with independent pO_2 measurements. Similar correlative experiments have been done [22, 37–41]; however, this is the first to assess the impact of thresholding various imaging metrics on tumor HFs. The dependence of tumor hypoxia quantification on metric and threshold choice is shown.

Three commonly used TBR thresholds (~1 in normal tissue) to define tumor hypoxia were compared: >1.2 [42–51], >1.3 [52–54], and >1.4 [9, 55]. Variation in median HFs for the same tumor depend on TBR threshold selection when compared to median HFs defined by pO_2 <5 mmHg. This suggests that certain TBR thresholds may provide an inaccurate HF that is different from physiologically meaningful hypoxia. To account for TBR inaccuracies, kinetic modeling can be applied on a voxel-by-voxel basis to

provide hypoxic heterogeneity information [19] and differentiate hypoxic (irreversible tracer accumulation) from normoxic regions (reversible tracer uptake) [56]. Mouse median HFs varied by up to a factor of 3 when defined by a TBR of >1.2, 1.3, or >1.4 (thresholds used in clinical studies [9, 52, 57–59]), when compared to those defined by kinetic parameters (k_3, 2TC K_i, and Patlak K_i). For M1, HF was 0 % (TBR >1.4) versus 33 % (k_3 > 0.004 min^{-1}). As TBR is a static measure, it provides a composite map of peripheral tracer clearance, tracer delivery, and clearance in the tumor, as well as irreversible tumor uptake due to hypoxia. This may explain the large variation in HFs and significant size differences when compared to kinetic modeling parameters. Although we expect the use of different thresholds to produce different HFs, in the clinic, this reality is often ignored and HFs are defined somewhat arbitrarily.

Despite the advantages, kinetic modeling remains imperfect for HF quantification. Aside from lengthy imaging protocols, the partial volume effect (PVE) still affects all kinetic modeling tumor HF measures (as it does for TBR especially for small tumors) and can impact the input function [21] and the shape of the TACs [19]. We showed a variation by up to a factor of 1.5 in median HF defined by k_3 compared to those defined by K_i (with either model). If the model had been constrained for noise, to calculate HFs defined by k_3, the difference between these volumes and those defined by K_i may be reduced [22]. However, we did not implement a constrained fit as we lacked sufficient data to adequately and precisely define the constrained values. In
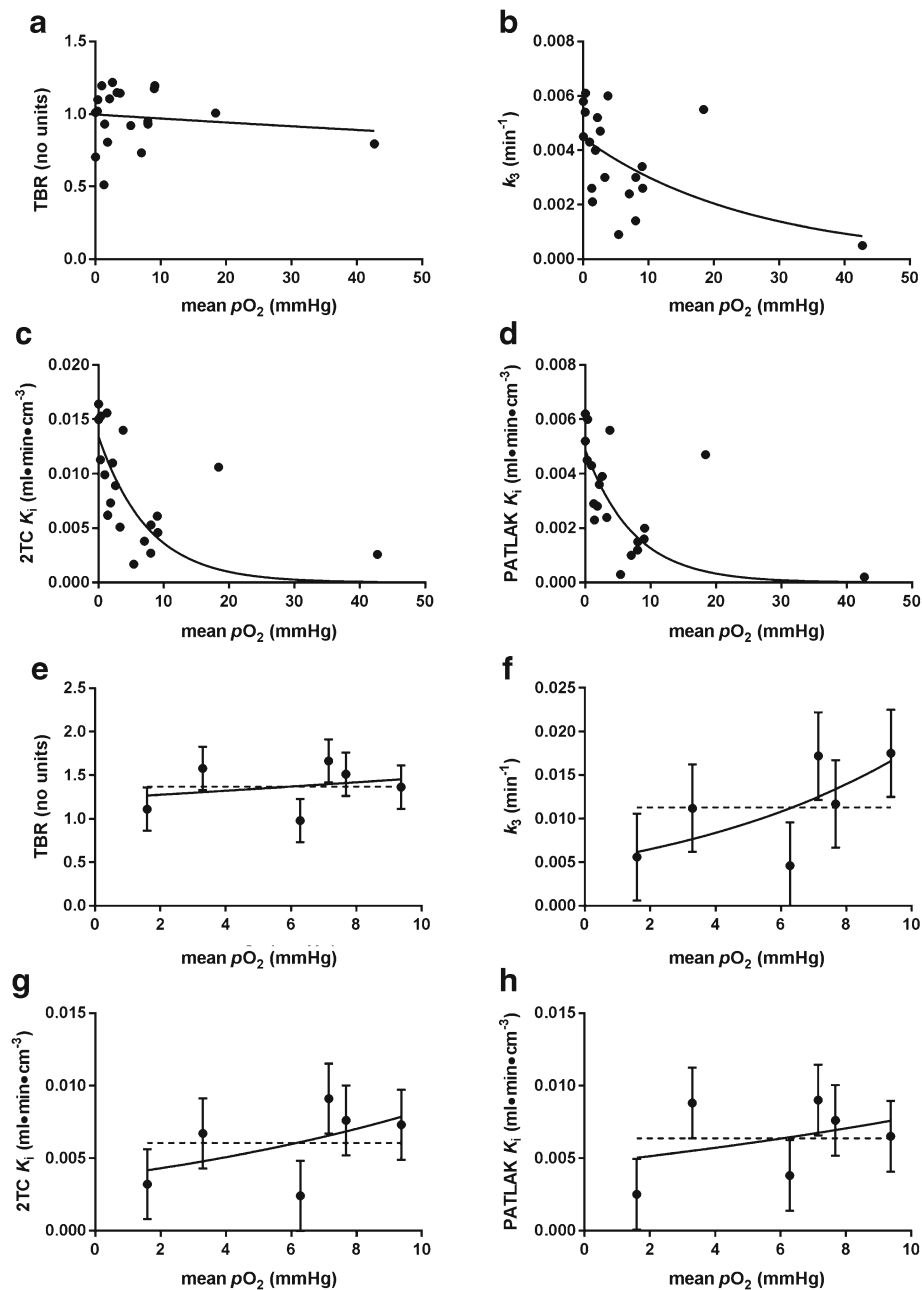
Fig. 4. **a** TBR, **b** k_3, **c** 2TC K_i, and **d** Patlak K_i as a function of independently measured partial oxygen pressure for a single mouse (M1) tumor described by $Y = Y0*\exp(K*X)$. (**e–h**) *Symbols* show mean tumor (*circle*) PET imaging metric and mean tumor pO_2 for each mouse (M1–M6). *Dashed lines* show the fit of a horizontal. A horizontal line through the data compared with *solid lines* indicating the fit of a nonlinear inverse-exponential described by $Y = Y0*\exp(K*X)$ for **e**, **f**, **g**, and **h**. *Error bars* are standard deviations of the mean for each [18F]FMISO metric.

addition, that there is no clear overestimation or underestimation of hypoxia using pO_2 compared to the various PET measurements. This could be due to the fact that PET resolution (1.5 mm) cannot directly capture all radiobiological relevant heterogeneity in tumor hypoxia, which occurs at a distance of 100–200 μm [60]. As [18F]FMISO uptake parameters all have steep gradient changes and considering the low resolution of PET, averaging of these values may have resulted in a loss of information. Also, the bioreduction of [18F]FMISO only exists over a finite range of pO_2 values (0–20 mmHg) and this may be a source for error as this range corresponds to varying levels of hypoxia i.e., severe or moderate and this information could be lost in the image [22, 35, 61].

As clinical practice moves towards the use of hypoxic quantification metrics, including kinetic parameters [62], it is
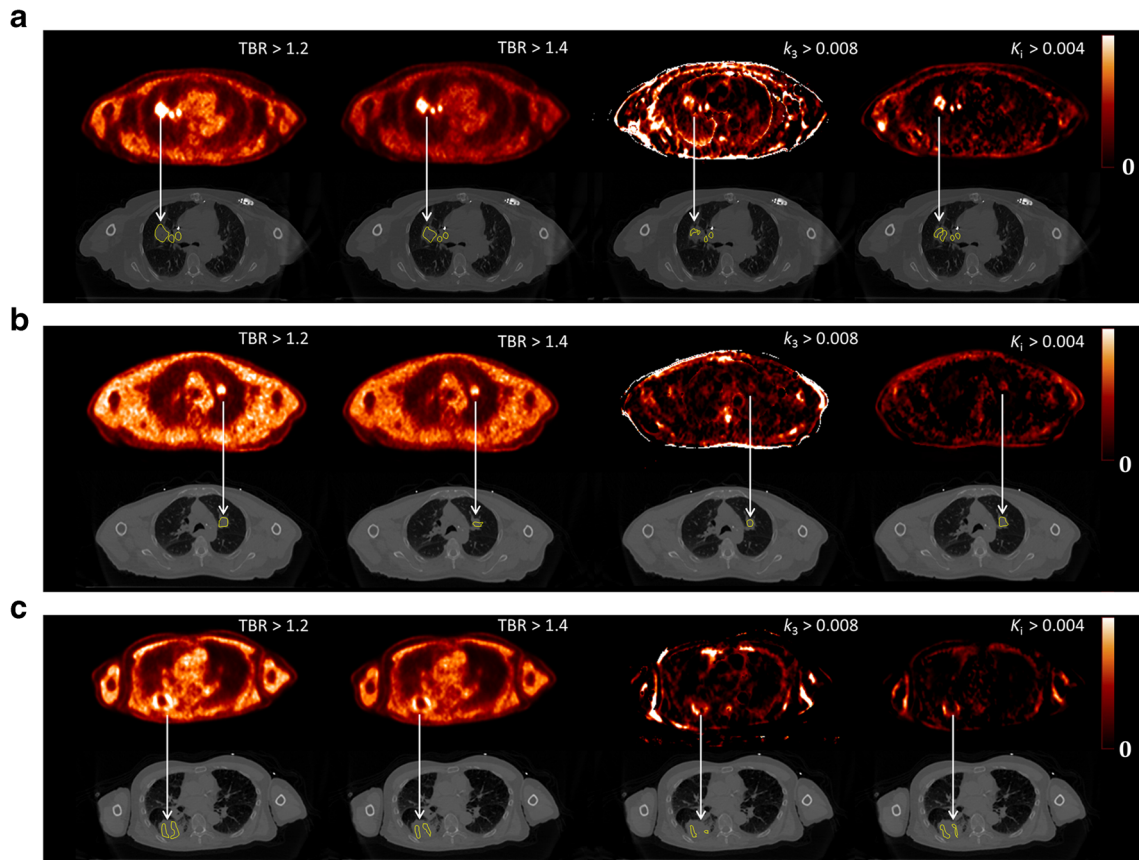
Fig. 5. Translation of tumor hypoxic volumes onto treatment planning CT. *Yellow contours* represent potential biological target volume (BTV) defined by [18F]FMISO PET to receive radiation dose escalation. Patients with early stage (I–II) NSCLC (tumor diameters of 4.1, 2.2, and 5.3 cm for patients A, B, and C) and were prescribed 10–18 Gy × 3 stereotactic radiation therapy. **a**, **b**, and **c** represent patients A, B, and C: [18F]FMISO PET image summed from 210 to 240 min post-injection, BTVs defined using tumor-to-blood (TBR) >1.2 and >1.4 and k_3 2TC image and K_i Patlak images for the same image slice and time frame. *Arrows* indicate tumor hypoxia, and *scale bar* on the right shows hypoxia as white.

critical to correctly interpret their physiological meaning to more accurately define HF and facilitate comparison of results across institutions. As highlighted by the change in HF with threshold in Fig. 5, inaccurate assessment of patient hypoxic status could make it challenging to stratify patients and overcome hypoxic radioresistance [26, 46, 50–53, 63].

To elucidate this, we correlated mean pO_2 values with imaging metrics for the same approximate spatial tumor volume (Fig. 3). The difference in kinetic parameter values for tumor and muscle was statistically significant ($p \leq 0.05$), but this was not the case with TBR. This is consistent with other studies that suggest TBR may not provide accurate hypoxic analysis [19] and others showing it may not correlate with pO_2 [64].

However, the voxel-by-voxel correlation was unclear between each imaging metric and pO_2 for the same approximate spatial area in most subjects with the exception of M1 (Fig. 4 a–d). We attribute this to a number of factors. First, Eppendorf pO_2 electrode is user-dependent [4] and spatial registration error may have resulted from deformation of the probe trajectory during measurements. Second, as HF is defined as viable tissue, macroscopic areas of necrosis (if

present in the tumor) do not affect the value of the HF fraction as defined by [18F]FMISO PET as these areas lack detectible uptake. However, a low pO_2 reading could be obtained in a necrotic region using the electrode and artificially lower the HF value [65]. Third, tumor ROI values were averaged to obtain representative pO_2 and [18F]FMISO uptake values to account for under-sampling and user- dependence of the pO_2 electrode [4] and poor tracer differentiation of hypoxic regions. Moreover, muscle histograms do contain values <20 mmHg and this may be a result of prolonged time under anesthesia and possible misplacement of the probe into nearby fascia or fatty tissue. Finally, of the six mice presented, CAIX staining was only performed on two of them; thus, we have limited knowledge of the necrotic fraction. Also, quantitative analysis of the CAIX staining results was challenging and suffered from severe undersampling. As a result, we decided to remove the IHC section from the manuscript.

Despite the aforementioned challenges, increased accuracy of tumor hypoxia quantification techniques in the clinical setting has the potential to improve cancer patient outcomes through (1) selective stratification to hypoxia-

targeted drug trials and (2) more optimal radiotherapy planning and delivery both aimed at overcoming treatment resistance. Inaccurate assessment of patient hypoxic status can make it challenging to stratify patients and overcome hypoxic radioresistance [46, 50–53, 63]. This has potentially significant implications for the clinical setting in the context of dose escalation for targeting hypoxic subvolumes or stratification of patients into subgroups for personalized hypoxia modification therapies. While our results do not demonstrate a clear statistical significance and none of the quantification strategies elucidate a clear and reliable correlation with pO_2, they are suggestive that tracer kinetics may provide an improved characterization of tumor hypoxia using [^{18}F]FMISO PET imaging and indicate a direction for future research.

Conclusions

Different PET imaging metrics and thresholds can result in substantially different tumor HF measurements. Our results suggest a direction for future studies without providing a statistically significant demonstration that tracer kinetic modeling has potential to improve quantification clinically. Future experiments are needed to provide more accurate imaging metrics and refine pO_2 measurement techniques to better quantify tumor hypoxia. Accurate hypoxia quantification techniques have the potential to impact patient treatment decisions and improve radiotherapy patient outcomes.

Compliance with Ethical Standards

Conflict of Interest

The authors declare that they have no conflict of interest.

References

1. Overgaard J (2011) Hypoxic modification of radiotherapy in squamous cell carcinoma of the head and neck—a systematic review and meta-analysis. Radiother Oncol 100:22–32
2. Hockel M, Schlenger K, Aral B et al (1996) Association between tumor hypoxia and malignant progression in advanced cancer of the uterine cervix. Cancer Res 56:4509–4515
3. Brizel DM, Scully SP, Harrelson JM et al (1996) Tumor oxygenation predicts for the likelihood of distant metastases in human soft tissue sarcoma. Cancer Res 56:941–943
4. Adam MF, Dorie MJ, Brown JM (1999) Oxygen tension measurements of tumors growing in mice. Int J Radiat Oncol Biol Phys 45:171–180
5. Kelada OJ, Carlson DJ (2014) Molecular imaging of tumor hypoxia with positron emission tomography. Radiat Res 181:335–349
6. Tatum JL, Kelloff GJ, Gillies RJ et al (2006) Hypoxia: importance in tumor biology, noninvasive measurement by imaging, and value of its measurement in the management of cancer therapy. Int J Radiat Biol 82:699–757
7. Ballinger JR (2001) Imaging hypoxia in tumors. Semin Nucl Med 31:321–329
8. Rasey JS, Koh WJ, Grierson JR et al (1989) Radiolabelled fluoromisonidazole as an imaging agent for tumor hypoxia. Int J Radiat Oncol Biol Phys 17:985–991
9. Koh WJ, Rasey JS, Evans ML et al (1992) Imaging of hypoxia in human tumors with [F-18]fluoromisonidazole. Int J Radiat Oncol Biol Phys 22:199–212
10. Valk PE, Mathis CA, Prados MD et al (1992) Hypoxia in human gliomas: demonstration by PET with fluorine-18-fluoromisonidazole. J Nucl Med 33:2133–2137
11. Rasey JS, Koh WJ, Evans ML et al (1996) Quantifying regional hypoxia in human tumors with positron emission tomography of [^{18}F]fluoromisonidazole: a pretherapy study of 37 patients. Int J Radiat Oncol Biol Phys 36:417–428
12. Rasey JS, Casciari JJ, Hofstrand PD et al (2000) Determining hypoxic fraction in a rat glioma by uptake of radiolabeled fluoromisonidazole. Radiat Res 153:84–92
13. Laubenbacher C, Schwaiger M (2000) The potential role of positron emission tomography in investigation of microenvironment blood perfusion and microenvironment of human tumors Eds. Molls M, Vaupel P. Berlin: springer.
14. Gagel B, Reinartz P, Dimartino E et al (2004) pO(2) polarography versus positron emission tomography ([^{18}F] fluoromisonidazole, [^{18}F]-2-fluoro-2′-deoxyglucose). An appraisal of radiotherapeutically relevant hypoxia. Strahlenther Onkol 180:616–622
15. Monnich D, Troost EG, Kaanders JH et al (2013) Correlation between tumor oxygenation and ^{18}F-fluoromisonidazole PET data simulated based on microvessel images. Acta Oncol 52:1308–1313
16. Chang J, Wen B, Kazanzides P et al (2009) A robotic system for ^{18}F-FMISO PET-guided intratumoral pO2 measurements. Med Phys 36:5301–5309
17. Monnich D, Troost EG, Kaanders JH et al (2011) Modelling and simulation of [^{18}F]fluoromisonidazole dynamics based on histology-derived microvessel maps. Phys Med Biol 56:2045–2057
18. Carson RE (2003) Tracer kinetic modelling in PET. In: Valk P, Bailey D, Townsend DW, Maisey MN (eds) Positron emission tomography: basic science and clinical practice. Springer, New York, pp 147–179
19. Thorwarth D, Eschmann SM, Paulsen F, Alber M (2005) A kinetic model for dynamic [^{18}F]-Fmiso PET data to analyse tumour hypoxia. Phys Med Biol 50:2209–2224
20. Kelly CJ, Brady M (2006) A model to simulate tumour oxygenation and dynamic [^{18}F]-Fmiso PET data. Phys Med Biol 51:5859–5873
21. Wang W, Georgi JC, Nehmeh SA et al (2009) Evaluation of a compartmental model for estimating tumor hypoxia via FMISO dynamic PET imaging. Phys Med Biol 54:3083–3099
22. Bartlett RM, Beattie BJ, Naryanan M et al (2012) Image-guided PO2 probe measurements correlated with parametric images derived from ^{18}F-fluoromisonidazole small-animal PET data in rats. J Nucl Med 53:1608–1615
23. Rockwell S (1977) In vivo-in vitro tumor systems: new models for studing the response of tumours to therapy. Lab Anim Sci 27:831–851
24. Moulder JE, Rockwell S (1984) Hypoxic fractions of solid tumors: experimental techniques, methods of analysis, and a survey of existing data. Int J Radiat Oncol Biol Phys 10:695–712
25. Kim EY, Liu Y, Akintujoye OM et al (2012) Preliminary studies with a new hypoxia-selective cytotoxin, KS119W, in vitro and in vivo. Radiat Res 178:126–137
26. Rischin D, Hicks RJ, Fisher R et al (2006) Prognostic significance of [^{18}F]-misonidazole positron emission tomography-detected tumor hypoxia in patients with advanced head and neck cancer randomly assigned to chemoradiation with or without tirapazamine: a substudy of Trans-Tasman Radiation Oncology Group Study 98.02. J Clin Oncol 24:2098–2104
27. Donnelly ET, Liu Y, Fatunmbi YO et al (2004) Effects of texaphyrins on the oxygenation of EMT6 mouse mammary tumors. Int J Radiat Oncol Biol Phys 58:1570–1576
28. Graves EE, Vilalta M, Cecic IK et al (2010) Hypoxia in models of lung cancer: implications for targeted therapeutics. Clin Cancer Res 16:4843–4852
29. Zheng MQ, Collier L, Bois F et al (2015) Synthesis of [^{18}F]FMISO in a flow-through microfluidic reactor: development and clinical application. Nucl Med Biol 42:578–584
30. Jenkinson M, Smith S (2001) A global optimisation method for robust affine registration of brain images. Med Image Anal 5:143–156

31. Jenkinson M, Bannister P, Brady M, Smith S (2002) Improved optimization for the robust and accurate linear registration and motion correction of brain images. NeuroImage 17:825–841

32. Patlak CS, Blasberg RG, Fenstermacher JD (1983) Graphical evaluation of blood-to-brain transfer constants from multiple-time uptake data. J Cereb Blood Flow Metab 3:1–7

33. Collingridge DR, Young WK, Vojnovic B et al (1997) Measurement of tumor oxygenation: a comparison between polarographic needle electrodes and a time-resolved luminescence-based optical sensor. Radiat Res 147:329–334

34. Wilcoxon F (1946) Individual comparisons of grouped data by ranking methods. J Econ Entomol 39:269

35. Urtasun RC, Chapman JD, Raleigh JA et al (1986) Binding of ^{3}H-misonidazole to solid human tumors as a measure of tumor hypoxia. Int J Radiat Oncol Biol Phys 12:1263–1267

36. Carlson DJ, Stewart RD, Semenenko VA (2006) Effects of oxygen on intrinsic radiation sensitivity: a test of the relationship between aerobic and hypoxic linear-quadratic (LQ) model parameters. Med Phys 33:3105–3115

37. Bejot R, Kersemans V, Kelly C et al (2010) Pre-clinical evaluation of a 3-nitro-1,2,4-triazole analogue of [^{18}F]FMISO as hypoxia-selective tracer for PET. Nucl Med Biol 37:565–575

38. Sorensen M, Horsman MR, Cumming P et al (2005) Effect of intratumoral heterogeneity in oxygenation status on FMISO PET, autoradiography, and electrode Po2 measurements in murine tumors. Int J Radiat Oncol Biol Phys 62:854–861

39. Valable S, Petit E, Roussel S et al (2011) Complementary information from magnetic resonance imaging and ^{18}F-fluoromisonidazole positron emission tomography in the assessment of the response to an antiangiogenic treatment in a rat brain tumor model. Nucl Med Biol 38:781–793

40. Bruehlmeier M, Kaser-Hotz B, Achermann R et al (2005) Measurement of tumor hypoxia in spontaneous canine sarcomas. Vet Radiol Ultrasound 46:348–354

41. Mortensen LS, Busk M, Nordsmark M et al (2011) Accessing radiation response using hypoxia PET imaging and oxygen sensitive electrodes: a preclinical study. Radiother Oncol 99:418–423

42. Szeto MD, Chakraborty G, Hadley J et al (2009) Quantitative metrics of net proliferation and invasion link biological aggressiveness assessed by MRI with hypoxia assessed by FMISO-PET in newly diagnosed glioblastomas. Cancer Res 69:4502–4509

43. Rajendran JG, Mankoff DA, O'Sullivan F et al (2004) Hypoxia and glucose metabolism in malignant tumors: evaluation by [^{18}F]fluoromisonidazole and [^{18}F]fluorodeoxyglucose positron emission tomography imaging. Clin Cancer Res 10:2245–2252

44. Swanson KR, Chakraborty G, Wang CH et al (2009) Complementary but distinct roles for MRI and ^{18}F-fluoromisonidazole PET in the assessment of human glioblastomas. J Nucl Med 50:36–44

45. Rajendran JG, Krohn KA (2005) Imaging hypoxia and angiogenesis in tumors. Radiol Clin N Am 43:169–187

46. Rajendran JG, Schwartz DL, O'Sullivan J et al (2006) Tumor hypoxia imaging with [F-18] fluoromisonidazole positron emission tomography in head and neck cancer. Clin Cancer Res 12:5435–5441

47. McKeage MJ, Jameson MB, Ramanathan RK et al (2012) PR-104 a bioreductive pre-prodrug combined with gemcitabine or docetaxel in a phase Ib study of patients with advanced solid tumours. BMC Cancer 12:496

48. Hugonnet F, Fournier L, Medioni J et al (2011) Metastatic renal cell carcinoma: relationship between initial metastasis hypoxia, change after 1 month's sunitinib, and therapeutic response: an ^{18}F-fluoromisonidazole PET/CT study. J Nucl Med 52:1048–1055

49. Kawai N, Maeda Y, Kudomi N et al (2011) Correlation of biological aggressiveness assessed by 11C-methionine PET and hypoxic burden assessed by ^{18}F-fluoromisonidazole PET in newly diagnosed glioblastoma. Eur J Nucl Med Mol Imaging 38:441–450

50. Dirix P, Vandecaveye V, De Keyzer F et al (2009) Dose painting in radiotherapy for head and neck squamous cell carcinoma: value of repeated functional imaging with (18)F-FDG PET, ^{18}F-fluoromisonidazole PET, diffusion-weighted MRI, and dynamic contrast-enhanced MRI. J Nucl Med 50:1020–1027

51. Nehmeh SA, Lee NY, Schroder H et al (2008) Reproducibility of intratumor distribution of ^{18}F-fluoromisonidazole in head and neck cancer. Int J Radiat Oncol Biol Phys 70:235–242

52. Lin Z, Mechalakos J, Nehmeh S et al (2008) The influence of changes in tumor hypoxia on dose-painting treatment plans based on ^{18}F-FMISO positron emission tomography. Int J Radiat Oncol Biol Phys 70:1219–1228

53. Lee NY, Mechalakos JG, Nehmeh S et al (2008) Fluorine-18-labeled fluoromisonidazole positron emission and computed tomography-guided intensity-modulated radiotherapy for head and neck cancer: a feasibility study. Int J Radiat Oncol Biol Phys 70:2–13

54. Kikuchi M, Yamane T, Shinohara S, et al. (2011) 18F–fluoromisonidazole positron emission tomography before treatment is a predictor of radiotherapy outcome and survival prognosis in patients with head and neck squamous cell carcinoma. Ann Nucl Med 9:625–633

55. Koh WJ, Bergman KS, Rasey JS et al (1995) Evaluation of oxygenation status during fractionated radiotherapy in human nonsmall cell lung cancers using [F-18]fluoromisonidazole positron emission tomography. Int J Radiat Oncol Biol Phys 33:391–398

56. Li F, Joergensen JT, Hansen AE, Kjaer A (2014) Kinetic modeling in PET imaging of hypoxia. Am J Nucl Med Mol Imaging 4:490–506

57. Hicks RJ, Rischin D, Fisher R et al (2005) Utility of FMISO PET in advanced head and neck cancer treated with chemoradiation incorporating a hypoxia-targeting chemotherapy agent. Eur J Nucl Med Mol Imaging 32:1384–1391

58. Thorwarth D, Eschmann SM, Scheiderbauer J et al (2005) Kinetic analysis of dynamic ^{18}F-fluoromisonidazole PET correlates with radiation treatment outcome in head-and-neck cancer. BMC Cancer 5:152

59. Thorwarth D, Eschmann SM, Holzner F et al (2006) Combined uptake of [^{18}F]FDG and [^{18}F]FMISO correlates with radiation therapy outcome in head-and-neck cancer patients. Radiother Oncol 80:151–156

60. Busk M, Horsman MR, Overgaard J (2008) Resolution in PET hypoxia imaging: voxel size matters. Acta Oncol 47:1201–1210

61. Koch CJ, Giandomenico AR, Iyengar CW (1993) Bioreductive metabolism of AF-2[2-(2-furyl)-3-(5-nitro-2-furyl)acrylamide] combined with 2-nitroimidazoles. Implications for use as hypoxic cell markers. Biochem Pharmacol 46:1029–1036

62. Askoxylakis V, Dinkel J, Eichinger M et al (2012) Multimodal hypoxia imaging and intensity modulated radiation therapy for unresectable non-small-cell lung cancer: the HIL trial. Radiat Oncol 7:157

63. Hendrickson K, Phillips M, Smith W et al (2011) Hypoxia imaging with [F-18] FMISO-PET in head and neck cancer: potential for guiding intensity modulated radiation therapy in overcoming hypoxia-induced treatment resistance. Radiother Oncol 101:369–375

64. Bentzen L, Keiding S, Nordsmark M et al (2003) Tumour oxygenation assessed by ^{18}F-fluoromisonidazole PET and polarographic needle electrodes in human soft tissue tumours. Radiother Oncol 67:339–344

65. Krohn KA, Link JM, Mason RP (2008) Molecular imaging of hypoxia. J Nucl Med 49(Suppl 2):129S–148S